

Band Gap and Electronic Structure of an Epitaxial, Semiconducting $\text{Cr}_{0.80}\text{Al}_{0.20}$ Thin Film

Z. Boekelheide,^{1,2,*} A. X. Gray,^{3,2} C. Papp,^{4,2} B. Balke,^{5,2} D. A. Stewart,⁶ S. Ueda,⁷ K. Kobayashi,⁷
F. Hellman,^{1,2} and C. S. Fadley^{3,2}

¹Department of Physics, University of California, Berkeley, Berkeley, California 94720, USA

²Materials Sciences Division, Lawrence Berkeley National Laboratory, Berkeley, California 94720, USA

³Department of Physics, University of California, Davis, Davis, California 95616, USA

⁴Lehrstuhl für Physikalische Chemie II, Universität Erlangen-Nürnberg, Egerlandstr. 3, 91058 Erlangen, Germany

⁵Institut für Anorganische und Analytische Chemie Johannes Gutenberg Universität, 55099 Mainz, Germany

⁶Cornell Nanoscale Facility, Cornell University, Ithaca, New York 14853 USA

⁷NIMS Beamline Station at SPring-8, National Institute for Materials Science, Hyogo 678-5148, Japan

(Received 22 August 2010; published 3 December 2010)

$\text{Cr}_{1-x}\text{Al}_x$ exhibits semiconducting behavior for $x = 0.15\text{--}0.26$. This Letter uses hard x-ray photoemission spectroscopy and density functional theory to further understand the semiconducting behavior. Photoemission measurements of an epitaxial $\text{Cr}_{0.80}\text{Al}_{0.20}$ thin film show several features in the valence band region, including a gap at the Fermi energy (E_F) for which the valence band edge is 95 ± 14 meV below E_F . Theory agrees well with the valence band measurements, and shows an incomplete gap at E_F due to the hole band at M shifting almost below E_F .

DOI: 10.1103/PhysRevLett.105.236404

PACS numbers: 71.20.Lp, 71.23.-k, 71.28.+d, 79.60.Bm

Intermetallic compounds containing transition metals and sp elements often form a gap at the Fermi energy (E_F) due to hybridization. This gap can be exploited for applications, making these compounds the subject of intense study. For example, intermetallic semiconductors are attractive for thermoelectric devices due to their typically small gaps and large Seebeck coefficients (e.g., ZrNiSn) [1]. In magnetic compounds, the gap is asymmetric with spin; if a gap occurs at E_F for one spin but not the other, the result is a half-metal (e.g., Co_2MnAl) [2]. Half-metals are important for spintronics circuits such as spin transistors and nonvolatile logic.

Compounds of the form A_2BD or A_3D , where A and B are transition metals and D is an sp element, typically crystallize in the ternary ($L2_1$) or binary ($D0_3$) full-Heusler structures. These compounds are usually ferro- or ferrimagnetic, with the magnetic moment well predicted by a Slater-Pauling counting scheme: $M = Z - 24$, where Z is the total number of valence electrons in the unit cell [3]. For $Z = 24$, there is no net magnetization and a gap in both the majority and minority spin density of states (DOS), resulting in a semiconducting gap (e.g., pseudogap in Fe_2VAI) [4]. This tunability and predictability of parameters with Z makes Heusler compounds an attractive class of materials to work with.

$\text{Cr}_3\text{Al}(\text{Cr}_{1-x}\text{Al}_x)$ with $x \approx 0.25$ is an exception to this scheme. According to the Slater-Pauling counting scheme $Z = 21$ so it should be a metal with $M = -3$. Instead, $\text{Cr}_{1-x}\text{Al}_x$ is found to be antiferromagnetic for $x = 0\text{--}0.50$. Cr is an antiferromagnet with a spin-density wave (SDW) incommensurate with the lattice. The addition of Al causes the SDW to become commensurate, i.e., a simple antiferromagnetic structure, for $x \geq 0.03$. For $x = 0.15\text{--}0.26$, the Cr magnetic moment reaches $1\mu_B$ with a high Néel temperature of about 800 K [5].

In the same range of x , $\text{Cr}_{1-x}\text{Al}_x$ displays semiconducting behavior not yet adequately explained by theory [6]. The gap has been estimated to be between 6 and 60 meV, making $\text{Cr}_{1-x}\text{Al}_x$ a narrow-gap semiconductor [7–9].

In this Letter, we probe the electronic structure of $\text{Cr}_{0.80}\text{Al}_{0.20}$ through hard x-ray photoemission spectroscopy (HXPS) and density functional theory (DFT). Hard x rays are advantageous over soft x rays due to enhanced bulk sensitivity and relatively enhanced photoionization cross section of s electrons [10,11].

HXPS was done on an epitaxial $\text{Cr}_{0.80}\text{Al}_{0.20}$ thin film and a pure Cr reference film. The concentration $x = 0.20$ was chosen due to its high resistivity (ρ). $\rho(2K)$ vs x is shown in Fig. 1 for a series of approximately 400 Å $\text{Cr}_{1-x}\text{Al}_x(001)/\text{MgO}(001)$ films. The inset shows $\rho(T)$ for a $\text{Cr}_{0.78}\text{Al}_{0.22}(001)/\text{MgO}(001)$ thin film, grown in the same batch as the sample used for HXPS.

The $\text{Cr}_{0.80}\text{Al}_{0.20}(001)$ sample was a 429 Å film, grown epitaxially on a 300 °C $\text{MgO}(001)$ substrate by codeposition of Cr from an e -beam source and Al from an effusion cell at a rate of 0.4 Å/s and a base pressure of 5×10^{-9} Torr. Epitaxy was verified *in situ* by reflection high energy electron diffraction (RHEED) which showed a streaky pattern and *ex situ* by x-ray diffraction (XRD) which showed only the bcc (001) orientation in a $\theta - 2\theta$ scan and fourfold symmetry of the (011) peak in an azimuthal scan at 45° from normal. The Cr sample was a sputtered, polycrystalline 2280 Å film grown on SiO_2 -coated Si at 350 °C with an Ar sputtering gas pressure of 0.75 mTorr. The SDW in Cr thin films is very sensitive to deposition conditions and these conditions yield bulklike behavior in both the resistivity and SDW state [12].

$\text{Cr}_{1-x}\text{Al}_x$ crystallizes on a bcc sublattice like the Heusler alloys, but $D0_3$ ordering has never been observed [13].

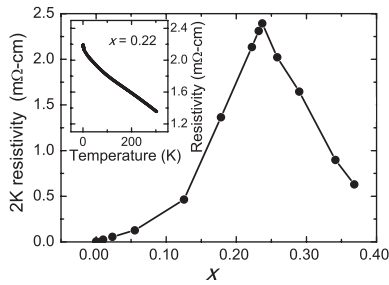


FIG. 1. ρ vs x for $\text{Cr}_{1-x}\text{Al}_x$ thin films at 2 K. Inset: $\rho(T)$ for $\text{Cr}_{0.78}\text{Al}_{0.22}$. Error bars smaller than symbols.

XRD suggests a random substitution of Al on the Cr lattice sites for $\text{Cr}_{1-x}\text{Al}_x$ in the range $x = 0$ – 0.26 ($x = 0$ – 0.35 for thin films) but a previous TEM study suggested that some non- DO_3 chemical ordering may occur for $\text{Cr}_{0.75}\text{Al}_{0.25}$, which should be studied further [14].

DFT calculations were done for Cr and a $\text{Cr}_{0.80}\text{Al}_{0.20}$ alloy using the AKAIKKR code, a full-potential DFT Green's function approach based on the Korringa-Kohn-Rostoker multiple-scattering technique [15–17]. The scalar relativistic approximation was used and disorder in the alloy was treated using the coherent potential approximation (CPA) [18,19]. The number of irreducible k points used for Brillouin zone integration was 3276. The generalized gradient approximation (GGA) was used to approximate the exchange-correlation energy [20], which results in equilibrium lattice constants very close to experiment (Cr: 2.882 Å calculated, 2.885 Å experimental; $\text{Cr}_{0.80}\text{Al}_{0.20}$: 2.935 Å calculated, 2.938 Å experimental [8]). The commensurate SDW was used for both $\text{Cr}_{0.80}\text{Al}_{0.20}$ and Cr. The incommensurate SDW in Cr not only requires a computationally difficult large unit cell but is, as of yet, not found to be the minimum energy state in current DFT calculations [21].

HXPS measurements were done at the undulator beam line BL15XU of SPring-8 with a fixed photon energy of 5956.4 eV. A VG Scienta R4000 hemispherical analyzer measured the kinetic energy of photoemitted electrons (PE electrons). Total energy resolution was 0.235 eV. A survey spectrum over an 800 eV binding energy range is shown in Fig. 2(a).

Hard x rays create high energy PE electrons which have relatively long mean free paths (MFPs). The inelastic MFP is calculated from the TPP-2M formula [22]: 72 Å (Cr) and 78 Å ($\text{Cr}_{0.80}\text{Al}_{0.20}$) for valence band (VB) PE electrons with 5956.4 eV kinetic energy. Cr and Al both form self-limiting surface oxides making bulk sensitivity especially important. The thickness of the surface oxide and residual adsorbent layers was modeled using the SESSA simulation package [23] and the relative intensities of the contaminant and sample core level peaks. Assuming an adsorbent CO layer and an oxide layer (Cr_2O_3 on Cr and Al_2O_3 on $\text{Cr}_{0.80}\text{Al}_{0.20}$) the simulation gives CO thicknesses of 4.95 and 3.85 Å and oxide thicknesses of 1.51 and 2.15 Å, respectively. The thickness of the surface layers is small

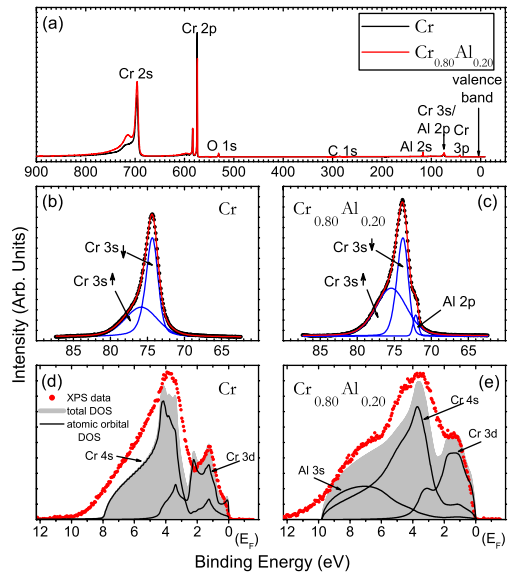


FIG. 2 (color online). (a) Broad spectrum HXPS survey; (b), (c) Cr 3s peak; (d), (e) Experimental and theoretical weighted VB.

compared to the PE electron inelastic MFPs, showing that the measurement probes the bulk electronic structure of the samples.

Figures 2(b) and 2(c) show the Cr 3s spectral region which displays multiplet splitting due to different binding energies of photoelectrons which are parallel and antiparallel to their atom's moment [24]. It is fit to a sum of two pseudo-Voigt peaks. For the $\text{Cr}_{0.80}\text{Al}_{0.20}$ sample the Al 2p peak falls nearby so it is shown as a sum of three pseudo-Voigt peaks. The integrated intensity of the broader multiplet peak is 1.82 times larger in $\text{Cr}_{0.80}\text{Al}_{0.20}$ than Cr, consistent with a larger Cr moment in $\text{Cr}_{0.80}\text{Al}_{0.20}$ (experimentally, $1.07\mu_B$ [5] vs $0.43\mu_B$ rms moment) [5,25]. DFT results in Cr moments of $1.6\mu_B$ in $\text{Cr}_{0.80}\text{Al}_{0.20}$ and $1.1\mu_B$ in Cr. The large calculated Cr moment is consistent with calculations in the literature and is due to overestimation of the moment by the GGA approximation [21]. The energy splitting between the multiplet peaks should also depend on moment; the splitting is 1.48 eV in Cr and 1.56 eV in $\text{Cr}_{0.80}\text{Al}_{0.20}$. This points to a larger moment in $\text{Cr}_{0.80}\text{Al}_{0.20}$ but the difference is not as large as expected. This may be due to our assumption of only two multiplet peaks.

Figures 2(d) and 2(e) depict the Shirley-background-subtracted VB spectra of Cr and $\text{Cr}_{0.80}\text{Al}_{0.20}$ along with the weighted DOS from the DFT calculations (the sum of the DOS of each atomic orbital weighted by its photoionization cross section). The neutral atom cross sections from Scofield [26] were used, corrected for the experimental geometry and nondipole effects [27,28].

The DOS in the VB spectra is dominated by Cr 3d, Cr 4s, and Al 3s contributions at 1.5, 4, and 7 eV, respectively. The energies of the features associated with each subshell from theory agree well with the experimental spectra. In the Cr spectra, the two large peaks associated with the Cr 3d and 4s orbitals are very sharp. In addition, the small

shoulder near E_F and the small bump at 2 eV can be attributed to peaks in the Cr $3d$ DOS, broadened by instrumental broadening. In $\text{Cr}_{0.80}\text{Al}_{0.20}$, the large Cr $3d$ and $4s$ peaks are significantly wider due to disorder broadening of the DOS. The tail extending to 10 eV is clearly attributed to the Al $3s$ orbital.

Figure 3(a) compares the experimental VBs of Cr and $\text{Cr}_{0.80}\text{Al}_{0.20}$ from Figs. 2(d) and 2(e) on the same scale. Figure 3(b) shows the VB edges in the region very close to E_F with a Au reference. The VB edges of Cr and $\text{Cr}_{0.80}\text{Al}_{0.20}$ appear shifted to lower energy than the Au VB edge. This is due to two effects: the recoil effect [29] and the semiconducting gap in $\text{Cr}_{0.80}\text{Al}_{0.20}$.

Au has an essentially constant DOS in the region of E_F so that the shape of the curve at E_F is simply the Fermi-Dirac distribution function at room temperature convoluted with a 0.235 eV Gaussian from instrumental broadening. Thus, Au is used to calibrate E_F . The Cr and Au spectra are normalized such that the slopes of the Gaussian dropoffs are equal; this is the case because they are both subject to the same broadening mechanisms. The $\text{Cr}_{0.80}\text{Al}_{0.20}$ spectrum is normalized relative to Cr such that the total electron occupation times cross section weighted, integrated intensities are equivalent.

The VB edge of Cr is shifted 35 ± 14 meV below that of Au. Cr has a metallic Fermi edge, so this shift is due to recoil. The expected recoil shift between Cr and Au is 46 meV, consistent with our measurement [30].

The $\text{Cr}_{0.80}\text{Al}_{0.20}$ VB edge is shifted 95 ± 14 meV below that of Cr. The recoil shift between Cr and $\text{Cr}_{0.80}\text{Al}_{0.20}$ is 7 meV, assuming an average atomic mass of 47 amu for $\text{Cr}_{0.80}\text{Al}_{0.20}$, within error of the gap measurement. Actually, the recoil shift should be less than 7 meV because the electrons near the VB edge of $\text{Cr}_{0.80}\text{Al}_{0.20}$ are primarily Cr-like (see Fig. 2). Thus, the 95 ± 14 meV shift is due to the semiconducting gap in $\text{Cr}_{0.80}\text{Al}_{0.20}$ causing a sharp dropoff in the DOS below E_F . This suggests that the VB edge is 95 ± 14 meV below E_F , putting a lower limit on the size of the semiconducting gap.

The observed gap in the $\text{Cr}_{0.80}\text{Al}_{0.20}$ VB spectrum is more striking when the weighting of atomic orbitals is considered because the s -orbital cross section is $16\times$ larger than the d at 5956.4 eV. In previous discussions of the semiconducting behavior in $\text{Cr}_{1-x}\text{Al}_x$, a qualitative explanation has been given in terms of the two $3d$ subbands in

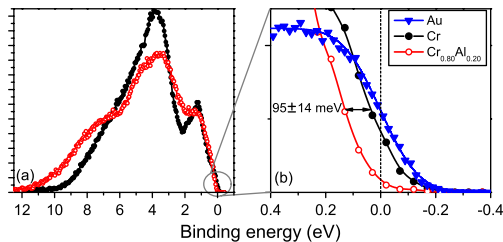


FIG. 3 (color online). (a) HXPS VB; (b) HXPS VB near E_F . Intensity scale is blown up $\times 10$ from (a).

Cr, one below and one above E_F , narrowing with addition of Al and creating a gap in the d band [8]. The problem with this explanation is that it does not consider the s electrons, which dominate electrical conduction, and therefore does not explain the semiconducting behavior. There are significantly more Cr $3d$ than Cr $4s$ electrons at E_F ; thus an enhanced $4s$ cross section is required for the photoemission measurement of the gap to measure both d and s electronic states at E_F . The theoretical weighted contributions are shown in Figs. 2(d) and 2(e). Previous XPS of $\text{Cr}_{1-x}\text{Al}_x$ used soft x rays (1500 eV) at which energy the s and d orbital cross sections are comparable; the previous work thus could not detect a gap in the s electrons [31]. Additionally, the soft x-ray study was susceptible to measuring surface states which could exist inside the bulk band gap.

The lower limit on the gap from the present measurement, 95 ± 14 meV, is comparable to but larger than previous estimates. Infrared reflectivity found a 40 meV gap in bulk $\text{Cr}_{0.81}\text{Al}_{0.19}$ and $\text{Cr}_{0.73}\text{Al}_{0.27}$; the difference could be due to different sample preparation or because infrared reflectivity can underestimate the gap due to exciton formation below the band edge [7]. Resistivity analyses estimated gaps of 6–60 meV for $\text{Cr}_{1-x}\text{Al}_x$, $x = 0.14$ – 0.28 , with the maximum gap occurring for 24 at. % Al [8]. These values are only approximate because the resistivity is not exponential in temperature.

DFT was used to generate the band structure of Cr and the Bloch spectral function (BSF) of $\text{Cr}_{0.80}\text{Al}_{0.20}$, shown in Fig. 4. In an alloy, disorder broadens the states into regions rather than bands, leading to the gray areas shown. The BSF is the k -projected DOS, $\mathcal{A}(E, \mathbf{k})$, which for a pure compound reduces to single valued dispersion relations $E_n(\mathbf{k})$ (the band structure).

The band structure of Cr in Fig. 4(a) shows states crossing E_F around M (holes) and X (electrons). Conduction in Cr occurs primarily by the holes around M [8]. The SDW opens a pseudogap in the regions Γ - M and R - Γ [32], which can be seen in the DOS in Fig. 4(c).

The BSF of $\text{Cr}_{0.80}\text{Al}_{0.20}$ in Fig. 4(b) shows Γ - M and R - Γ are still gapped due to the SDW. In addition, the hole band around M is shifted almost entirely below E_F , which should decrease conductivity due to a high effective mass and higher likelihood of localization as well as a lower DOS (E_F). This explains previous Hall effect data showing conduction switching from holes in pure Cr to electrons for $x \geq 0.15$ [8].

The DOS of Cr and $\text{Cr}_{0.80}\text{Al}_{0.20}$ are shown in Figs. 4(c) and 4(d), with 4(e) comparing the DOS near E_F . In $\text{Cr}_{0.80}\text{Al}_{0.20}$, the shift of the holes at M leads to a sharp dropoff in states just below E_F , as suggested by Fig. 3. The DOS (E_F) is much smaller than that of Cr, but still nonzero. It is possible that the gap leading to the semiconducting transport behavior and photoemission results is not a complete gap and a few states remain at E_F ; Fig. 3 is compatible with this possibility since a small but finite intensity is observed at zero binding energy. Previous

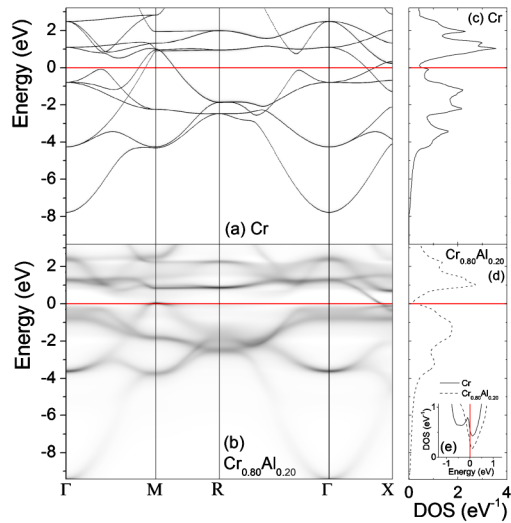


FIG. 4 (color online). (a) Cr band structure; (b) $\text{Cr}_{0.80}\text{Al}_{0.20}$ BSF; (c),(d) DOS; (e) DOS near EF.

results are also consistent with an incomplete gap, such as resistivity which is not exponential in temperature [8,9], an infrared “gap” showing finite reflectivity in the DC limit [7], and a nonzero electronic contribution to the specific heat [33].

DFT is thus largely consistent with the experimental data. However, some details remain to be explained: the calculated DOS (E_F) for $\text{Cr}_{0.80}\text{Al}_{0.20}$, while decreased compared to Cr, is larger than expected from the previously measured electronic contribution to the specific heat [33]. In addition, the $\text{Cr}_{0.80}\text{Al}_{0.20}$ DOS in the region near E_F , when convoluted to simulate experimental broadening, does not reproduce the observed 95 meV VB edge shift but falls much closer to the Cr DOS. DFT is known to underestimate the band gap of materials [34]; thus, it is possible that in the real $\text{Cr}_{0.80}\text{Al}_{0.20}$ material the holes at M are completely shifted below E_F , widening the gap and sharpening the DOS dropoff. In addition, if an ordered Cr_3Al structure exists, as has been speculated [14], it would have a different band structure which could have sharp features near E_F .

In summary, a gap is observed in $\text{Cr}_{0.80}\text{Al}_{0.20}$ by HXPS, with the VB edge 95 ± 14 meV below E_F . HXPS provided advantages over soft x-ray photoemission such as decreased sensitivity to surface states and a relatively increased photoionization cross section for s states, so the measurement truly reflects a gap in the bulk conducting s states and not simply a splitting of two d subbands.

DFT agrees well with the HXPS VB spectra. It shows that the primary carriers in Cr, the holes around M , are shifted almost entirely below E_F in $\text{Cr}_{0.80}\text{Al}_{0.20}$. It shows an incomplete gap in $\text{Cr}_{0.80}\text{Al}_{0.20}$, with a small number of states at E_F ; this is consistent with the photoemission and resistivity results. Future work will investigate the possibility of an ordered structure.

This work was supported by the U.S. Department of Energy under Contract No. DE-AC02-05CH11231 and the

Nanotechnology Network Project, MEXT, Japan. C. Papp and B. Balke thank the Humboldt foundation for support. Calculations were done at the Cornell Nanoscale Facility, part of the National Nanotechnology Infrastructure Network (NNIN) funded by the NSF. HXPS experiments were approved by NIMS Beamline Station (Proposal No. 2009A4906).

*zboekelheide@berkeley.edu

- [1] C. Uher *et al.*, *Phys. Rev. B* **59**, 8615 (1999).
- [2] J. Kübler, A. R. Williams, and C. B. Sommers, *Phys. Rev. B* **28**, 1745 (1983).
- [3] I. Galanakis *et al.*, *Phys. Status Solidi A* **205**, 1036 (2008).
- [4] Y. Nishino *et al.*, *Phys. Rev. Lett.* **79**, 1909 (1997).
- [5] E. Fawcett *et al.*, *Rev. Mod. Phys.* **66**, 25 (1994).
- [6] H. Akai and J. Kanamori, *J. Phys. Soc. Jpn.* **54**, 3537 (1985).
- [7] M. A. Lind and J. L. Stanford, *J. Phys. Soc. Jpn.* **53**, 4029 (1984).
- [8] D. J. Chakrabarti and P. A. Beck, *J. Phys. Chem. Solids* **32**, 1609 (1971).
- [9] L. V. Nomerovannaya and V. A. Rassokhin, *Phys. Status Solidi A* **79**, 87 (1983).
- [10] K. Kobayashi *et al.*, *Appl. Phys. Lett.* **83**, 1005 (2003).
- [11] K. Kobayashi, *Nucl. Instrum. Methods Phys. Res., Sect. A* **601**, 32 (2009).
- [12] Z. Boekelheide, E. Helgren, and F. Hellman, *Phys. Rev. B* **76**, 224429 (2007).
- [13] J. L. Murray, *J. Phase Equilib.* **19**, 367 (1998).
- [14] F. J. A. den Broeder *et al.*, *Phys. Status Solidi A* **67**, 233 (1981).
- [15] <http://sham.phys.sci.osaka-u.ac.jp/kkr/>.
- [16] J. Koringa, *Physica (Amsterdam)* **13**, 392 (1947).
- [17] W. Kohn and N. Rostoker, *Phys. Rev.* **94**, 1111 (1954).
- [18] P. Soven, *Phys. Rev.* **156**, 809 (1967).
- [19] H. Akai, *J. Phys. Condens. Matter* **1**, 8045 (1989).
- [20] J. P. Perdew *et al.*, *Phys. Rev. B* **46**, 6671 (1992).
- [21] R. Hafner *et al.*, *Phys. Rev. B* **65**, 184432 (2002).
- [22] S. Tanuma, C. J. Powell, and D. R. Penn, *Surf. Interface Anal.* **37**, 1 (2005).
- [23] W. Smekal, W. S. M. Werner, and C. J. Powell, *Surf. Interface Anal.* **37**, 1059 (2005).
- [24] L. E. Klebanoff and D. A. Shirley, *Phys. Rev. B* **33**, 5301 (1986).
- [25] The SDW has $0.43\mu_B$ rms and $0.62\mu_B$ peak moment.
- [26] J. H. Scofield, Tech. Rep., LLNL Report No. UCRL-51326, 1973.
- [27] M. B. Trzhaskovskaya, V. I. Nefedov, and V. G. Yarzhevsky, *At. Data Nucl. Data Tables* **77**, 97 (2001).
- [28] M. B. Trzhaskovskaya *et al.*, *At. Data Nucl. Data Tables* **92**, 245 (2006).
- [29] Y. Takata *et al.*, *Phys. Rev. Lett.* **101**, 137601 (2008).
- [30] $\Delta E_{\text{recoil}}^{\text{Cr-Au}} = \left(\frac{m_e}{M_{\text{Cr}}} - \frac{m_e}{M_{\text{Au}}}\right) E_{\text{kinetic}}$.
- [31] K. Ławniczak-Jabłńska *et al.*, *Phys. Status Solidi B* **123**, 627 (1984).
- [32] E. Fawcett, *Rev. Mod. Phys.* **60**, 209 (1988).
- [33] N. Pessall *et al.*, *J. Phys. Chem. Solids* **25**, 993 (1964).
- [34] R. M. Martin, *Electronic Structure: Basic Theory and Practical Methods* (Cambridge University Press, Cambridge, U.K., 2005).